Article:
Zhang, Zhihong, Bai, Lu, Ren, Peng et al. (1 more author) (2016) High-order graph matching kernel for early carcinoma EUS image classification. Multimedia Tools and Applications. 3993–4012. ISSN: 1573-7721

https://doi.org/10.1007/s11042-015-3108-1

Noname manuscript No.
(will be inserted by the editor)

High-Order Graph Matching Kernel for Early Carcinoma EUS Image Classification

Zhihong Zhang [1] · **Lu Bai** [3] · **Peng Ren** [2] · **Edwin R. Hancock** [4]

Received: date / Accepted: date

Abstract Endoscopic ultrasonography (EUS) is limited by variability in the examiner's subjective interpretation to differentiate between normal, leiomyoma of esophagus and early esophageal carcinoma. By using information otherwise discarded by conventional EUS systems, quantitative spectral analysis of the raw pixels (picture elements) underlying EUS image enables lesions to be characterized more objectively. In this paper, we propose to represent texture features of early esophageal carcinoma in EUS images as a graph by expressing pixels as nodes and similarity between the gray-level or local features of the EUS image as edges. Then, similarity measurements such as a high-order graph matching kernel can be constructed so as to provide an objective quantification of the properties of the texture features of early esophageal carcinoma in EUS images. This is in terms of the topology and connectivity of the analyzed graphs. Because such properties are directly related to the structure of early esophageal carcinoma lesions in EUS images, they can be used as features for characterizing and classifying early esophageal carcinoma. Finally, we use a refined SVM model based on the new high-order graph matching kernel, resulting an optimal prediction of the types of esophageal lesions. A 10-fold cross validation strategy is employed to evaluate the classification performance. After multiple computer runs of the new kernel SVM model, the overall accuracy for the diagnosis between normal, leiomyoma of esophagus and early esophageal carcinoma was 93%. Moreover, for the diagnosis of early esophageal carcinoma, the average accuracy, sensitivity, specificity, positive predictive value, and negative predictive value were 89.4%, 94%, 95%, 89%,

Corresponding author: Peng Ren, renpenghit@126.com

[1] Software school, Xiamen University, Xiamen, Fujian, China
[2] College of Information and Control Engineering, China University of Petroleum, Qingdao, China.
[3] School of Information,Central University of Finance and Economics, Beijing, China
[4] Department of Computer Science, University of York, York, UK

and 97% respectively. The area under all the three ROC curves were close to 1.

Keywords Graph matching · Kernel · Endoscopic ultrasonography (EUS) image classification

1 Introduction

Digestive system malignant tumors are common diseases for the human, and so the diagnosis of gastrointestinal early carcinoma is very important for patient prognosis. This remains a difficult task, even for well-trained specialists. Since its introduction in the 1980s, EUS has been established as a more accurate imaging procedure compared with alternative imaging methods in the diagnosis and staging of gastrointestinal malignant tumors. The greatest advantages of EUS are the visualization of the esophageal wall layers as well as a guided biopsy of the specimen. The determination of the depth of tumor invasion using EUS produces a 'five-layer' bright-dark-bright-dark-bright image of the esophageal wall (see Fig.1(b)): the first layer represents the superficial mucosa, the second layer corresponds to the mucosa, the third layer to the submucosa, the fourth layer the muscularis propria, and the fifth layer the adventitia. Early esophageal cancer is often visualized as hypoechoic disruption of the first three wall layers (see Fig.1(d)). However, EUS is usually limited by the variability of the examiners' subjective interpretation of images, and the yield of EUS-FNA may be affected by technical limitations and tumor related factors. In addition, biopsies are highly required because of the inability to specify target tumor cells, and this can result in complications attributed directly to the procedure. Thus, there is an urgent need for new technologies complementary to EUS for the diagnosis of early carcinoma. In particular, a better differential diagnostic system is needed to assist endoscopists in their decision making process and to guide EUS-FNA. Moreover, the methods can be used to distinguish Crohn's disease, intestinal tuberculosis, white plug's diseases and intestinal lymphoma.

Texture analysis is a basic issue in digital image processing (DIP) and computer vision. Texture features are helpful for the diagnosis of several diseases in clinical practice, and the potential of sonographic texture analysis to improve tumor diagnosis has already been demonstrated [1–3]. However, few reports exist regarding their use for EUS image classification. For the diagnosis of early esophageal carcinoma, research using DIP and pattern recognition even remains rare. For the diagnosis of pancreatic cancer, there are three reports [4–6] of successfully using neural network analysis of EUS images to differentiate pancreatic cancer from non-cancer. Das et al [5] reported high sensitivity (93%) and specificity (92%), with excellent positive predictive values (87%) and negative predictive values (96%). Loren et al [9] investigated the feasibility of a computer-assisted evaluation of lymph nodes detected by EUS in patients with esophageal carcinoma. Olowe et al [10] also applied quantitative

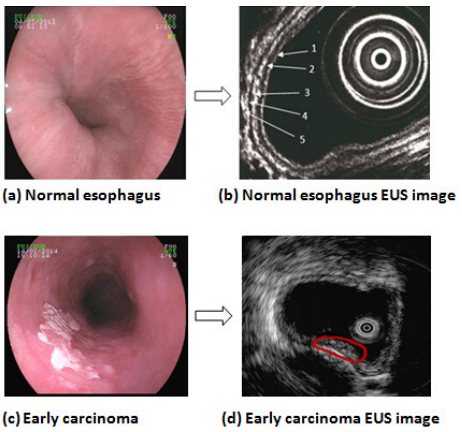

Fig. 1 EUS images of normal esophagus and early carcinoma

analysis of the raw RF spectrum of the backscattered ultrasound to determine the feasibility of differentiating benign and malignant mediastinal and abdonimal lymph nodes.

Another variation and application of EUS image analysis was based on a support vector machine (SVM), which is one a successful kernel method that learns the examples to assign labels to objects [11]. For example, two recent studies [13] [14] utilized a simple SVM classification models for the differential diagnosis of pancreatic cancer and chronic pancreatitis. The typical SVM method which only uses predefined standard kernel functions to measure the similarity of two objects. In our case, the source of data is EUS images [24]. However, standard kernel functions such as Gaussian or polynomial kernels are rather limited for processing complex structured data such as EUS images, and this may lead to a substantial loss of useful information. Therefore, further refinements of the SVM method with a new kernel function could increase the accuracy of the EUS diagnosis of tumors [13].

Digital images consist of pixels (picture elements), which are the basic elements that compose a 2-dimensional picture. In order to extract useful information in digital image analysis, the distribution and spatial variation of pixels is computed using texture analysis. Generally speaking, textures are complex visual patterns composed of entities, or sub-patterns. Texture can be considered as a group of repeated similarities relations on a image [15]. Thus the definition of a texture pattern must take into account not only the isolated primitives, but also the relations among pixels and their neighbors[18]. Consequently, texture characterization and identification requires a methodology capable of expressing the context surrounding each pixel, thus connecting local and global texture characteristics. Graph theory lends itself naturally to the analysis of the spatial relationship that exist in texture.

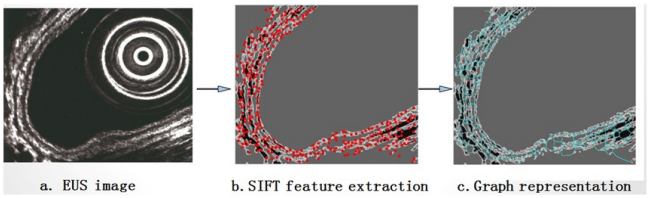

Fig. 2 Graph-based representation of EUS image

In this paper, we aim to represent texture features of early esophageal carcinoma in EUS images using graphs and expressing pixels as nodes and similarity between the gray-level or local features of the EUS image as weighted edges. Measurements obtained by means of a high-order graph matching kernel function can be constructed so as to provide an objective quantification of the properties of the texture features. For early esophageal carcinoma in EUS images this is in terms of the topology and connectivity of the analyzed graphs. Because such properties are directly related to the structure of early esophageal carcinoma lesions in EUS images, they can be used as features for characterizing and classifying early esophageal carcinoma. More specifically, there are three novel ingredients in our method. First, a graph based EUS image representation is proposed, where each node represents a key point detected by the SIFT algorithm (see Fig.2(b))[19]. Edges describe spatial relationships between different SIFT key points(see Fig.2(c)). The graph structure encodes information about key points located in a certain position of an image. Secondly, once the graph representation is obtained, we formulate the EUS image classification as a high-order graph matching problem. More specifically, we first develop an h-layer depth-based representations for a graph, which is effected by measuring the Shannon entropies [20] of a family of K-layer expansion subgraphs derived from a vertex of the graph. The depth-based representation characterizes graphs in terms of a high dimensional reformulation of the way in which the complexity of the graph changes with the depth from its perimeter. Based on the new representation, we first perform feature-based matching for EUS images. This results in a coarse feature point mapping with certain mismatches because the feature-based matching methods may neglect the spatial correlations between feature points. We thus develop a high-order graph matching scheme (referred to as hypergraph matching), which encodes spatial correlations as hyperedges which can be used for identifying the mismatches in the coarse matching results. Spatially inconsistent matches are then rejected from the refined matching results. Finally, we develop a high-order graph matching kernel and refine the SVM classifier using this new kernel. In summary, our method may offer four advantages:

(1) It allows an objective quantification of the lesion properties and offers information complementary to conventional EUS imaging;

(2) Unlike feature-based matching methods which neglect the spatial correlations between feature points, our method refines matched feature point

pairs using higher order spatial constraints expressed in terms of a high-order graph matching formulation. Furthermore, compared with alternative high-order graph matching methods, which are computationally expensive, our method reduces the computational complexity by taking advantages of the matching results obtained from feature-based matching. It achieves high efficiency in operation;
(3) Our high-order graph matching framework(referred to as hypergraph matching) is robust to scale variation because the hypergraphs characterize higher order spatial correlations which are scale invariant;
(4) The refinement of SVM model using an improved kernel better differentiate between normal, leiomyoma of esophagus and early esophageal carcinoma.

2 Patients

The protocol used in this study was reviewed and approved by the Institutional Review Board of the Zhongshan Hospital affiliated with Xiamen University, Xiamen, Fujian, China. From December 2011 to July 2014, a total of 1210 EUS examinations were performed at the Department of Gastroenterology, Zhongshan Hospital. Among this group, we randomly selected 66 patients with early esophageal cancer(mean age 53 years; age range 21-87 years; 32 male and 34 female). The diagnoses obtained by EUS were further verified by biopsy. To avoid selection bias, we excluded patients who had no early esophageal cancer over the study period. Patients with pancreas and gall bladder lesions or masses were also excluded. In total 91 patients (mean age 42 years; age range 32-75 years; 39 male and 52 female) who had no history of cancer (ie, EUS images of corresponding parts presented with a normal anatomical structure of the esophageal tract) were randomly selected and included as controls to describe the appearance of the healthy gastrointestine. None of the control studies had a history of pancreatic disease, symptoms of maldigestion, a history of alcohol abuse, or elevated serum levels of pancreatic enzymes. None of them was a smoker. All the EUS images obtained were processed and analyzed.

3 An Overview of Framework for EUS Image Classification

Figure 3 shows an overview of the proposed framework for EUS image classification. From the preprocessed EUS images, we first establish a graph from each ROI (region of interest). For each graph, the structure is characterized using depth-based representation [7]. The advantage of using the depth-based representation to characterize graphs is that it not only reflects dominant depth complexity information around the vertex for a graph but also represents each vertex in a high dimensional space. This is because the depth-based representation for a graph encapsulates information flow from the each vertex to the global graph using entropy measures. In other words, the depth-based representation reflect rich graph characteristics, and provides us an elegant way of

evaluating the correspondence between a pair of vertices between two graphs. Using the depth based representation of a graph, our framework takes first-order feature point matching results as the coarse matching results. Then we have conducted high-order feature point matching (referred to as hypergraph matching) for rejecting mismatches and thus obtained the refined correspondences. Based the matching results, a kernel is constructed. The kernel matrix is then used to train the SVM classifier.

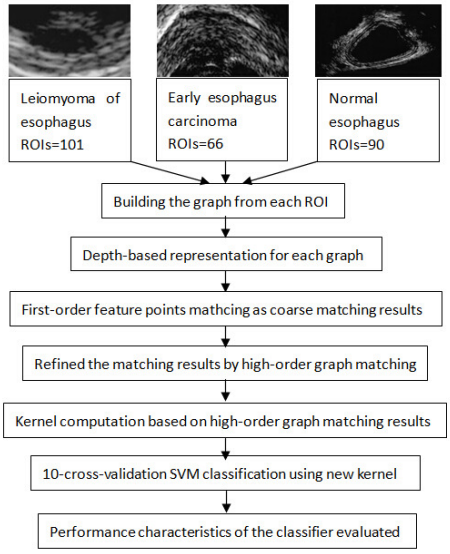

Fig. 3 Schematic diagram of the proposed classification framework

4 Depth-based Representations for EUS Images

An EUS image is represented by a graph $G(V, E)$ whose nodes represent the features selected using the SIFT algorithm [19] and nodes are connected based on the relative neighborhood graph (RNG). When graphs are obtained, the analysis of texture is converted to analysis a graph. Thus many graph-based algorithms could be employed. Here, we exploit the graph structure by characterising its high dimensional depth-based complexity information. The detail of process is as follows:

For an undirected graph $G(V, E)$ the shortest path $S_G(v, u)$ between a pair of vertices v and u can be computed by using Dijkstra algorithm. The matrix S_G whose element $S_G(v, u)$ represents the shortest path length between v and u is referred to as the shortest path matrix for G. Let N_v^K be a subset of

V satisfying $N_v^K = \{u \in V \mid S_G(v,u) \leq K\}$. For G, the K-layer expansion subgraph $\mathcal{G}_v^K(\mathcal{V}_v^K;\mathcal{E}_v^K)$ around vertex v is

$$\begin{cases} \mathcal{V}_v^K &= \{u \in N_v^K\}; \\ \mathcal{E}_v^K &= \{(u,v) \subset N_v^K \mid (u,v) \in E\}. \end{cases} \tag{1}$$

Let L_{max} be the greatest length of the shortest paths from v to the remaining vertices of $G(V,E)$. If $L_v \geq L_{max}$, then the L_v-layer expansion subgraph is $G(V,E)$ itself.

4.1 The Shannon Entropy of A Graph

We compute the Shannon entropy of a graph based on steady state random walks on the graph. Consider a graph $G(V,E)$ where V denotes the set of vertices and $E \subseteq V \times V$ denotes the set of undirected edges. The adjacency matrix A for $G(V,E)$ is a symmetric $|V| \times |V|$ matrix with the (v,u)th entry

$$A(v,u) = \begin{cases} 1 \text{ if} (v,u) \in E; \\ 0 \text{ otherwise.} \end{cases} \tag{2}$$

The vertex degree matrix of $G(V,E)$ is a diagonal matrix D whose vth diagonal element is given by $D(v,v) = d(v) = \sum_{u \in V} A(v,u)$. As a result, the probability of a steady state random walk on $G(V,E)$ visiting vertex v is $P_G(v) = d(v)/\sum_{u \in V} d(u)$. The Shannon entropy of $G(V,E)$ associated with the steady state random walk is

$$H_S(G) = -\sum_{v \in V} P_G(v) \log P_G(v). \tag{3}$$

4.2 The h-layer Depth-based Representation for A Graph

For a graph $G(V,E)$ and a vertex $v \in V$, the h-layer depth-based representation around v is a h dimensional vector

$$D_G^h(v) = [H_S(\mathcal{G}_v^1), \cdots, H_S(\mathcal{G}_v^K), \cdots, H_S(\mathcal{G}_v^h)]^T \tag{4}$$

where h ($h \leq L_v$) is the length of the shortest paths from v to other vertices in $G(V,E)$, $\mathcal{G}_v^K(\mathcal{V}_v^K;\mathcal{E}_v^K)$ ($K \leq h$) is the K-layer expansion subgraph of $G(V,E)$ around v, and $H_S(\mathcal{G}_v^K)$ is the Shannon entropy of $\mathcal{G}_v^K$ and is defined in Eq.(3).

The h-layer depth-based representation $D_G^h(v)$ characterizes the depth-based complexity of $G(V,E)$ with regard to the vertex v in a h dimensional feature space. It captures the rich depth-based complexity characteristics of substructures around the vertex v in terms of the entropies of the K-layer expansion subgraphs with K increasing from 1 to h. In contrast, the existing graph kernels in the literatures [21,22] tend to compute similarities on global subgraphs of limited sizes and can only capture restricted characteristics of graphs.

5 High-order graph matching for refining feature correspondences between two EUS images

In order to combine the merits of first-order feature point matching method and high-order feature matching method, we first extract feature points for each EUS image using the SIFT algorithm [19] and characterize each graph with the h-layer depth-based representation [7]. Then, we apply the first-order feature point matching method previously developed in [28,29] to obtain the initial matching results and hypergraphs based on the first-order feature matching results. Then, we use the high order structural refinement to update the initial matching results. Fig. 4 shows the framework of our hypergraph-based feature correspondence refinement method for EUS image databases.

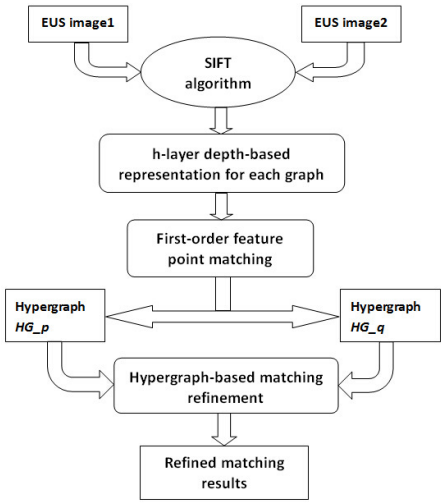

Fig. 4 The hypergraph matching framework for EUS images feature correspondences.

5.1 First-order Feature Point Matching

We develop a matching method similar to that introduced in [12] for point set matching, which computes an affinity matrix in terms of the distances between points. We thus obtain the initial matching results between two EUS images. In our work, for a vertex p of $G(V,E)$, we treat the h-layer depth-based representations $D_G^h(p)$ as the feature vector associated with p. We use the Euclidean distance between the depth-based representations $D_{G_p}^h(p_i)$ and $D_{G_q}^h(q_j)$ as the distance measure between the vertices p_i and q_j of graphs $G_p(V_p,E_p)$ and $G_q(V_q,E_q)$, respectively. The affinity matrix element $R(i,j)$ is

defined as

$$R(i,j) = \sqrt{[D^h_{G_p}(p_i) - D^h_{G_q}(q_j)]^T [D^h_{G_p}(p_i) - D^h_{G_q}(q_j)]}. \quad (5)$$

where R is a $|V_p| \times |V_q|$ matrix. The element $R(i,j)$ represents the dissimilarity between the vertex p_i in $G_p(V_p, E_p)$ and the vertex q_j in $G_q(V_q, E_q)$. The rows of $R(i,j)$ index the vertices of $G_p(V_p, E_p)$, and the columns index the vertices of $G_q(V_q, E_q)$. If $R(i,j)$ is the smallest element both in row i and in column j, there should be a one-to-one correspondence between the vertex p_i of G_p and the vertex q_j of G_q. We record the state of correspondence using the correspondence matrix $C \in \{0,1\}^{|V_p||V_q|}$ satisfying

$$C(i,j) = \begin{cases} 1 \text{ if } R(i,j) \text{ is the smallest element} \\ \quad \text{both in row } i \text{ and in column } j; \\ 0 \text{ otherwise.} \end{cases} \quad (6)$$

Eq.(6) implies that if $C(i,j) = 1$, the vertices p_i and q_j are matched. Note that, in row i or column j there may be two or more elements satisfying Eq.(6). In other words, for a pair of graphs, a vertex from a graph may have two or more matched vertices from the other graph. To assign a vertex one matched vertex at most, we update the matrix C by employing the Hungarian method that is widely used for solving the assignment problem (e.g., the bipartite graph matching problem) in polynomial time [30]. Here the matrix $C \in \{0,1\}^{|V_p||V_q|}$ can be seen as the incidence matrix of a bipartite graph $G_{pq}(V_p, V_q, E_{pq})$, where V_p and V_q are the two partition sets and E_{pq} is the edge set. By computing the Hungarian algorithm on the incidence matrix $C \in \{0,1\}^{|V_p||V_q|}$ (i.e., the correspondence matrix of G_p and G_q) of the bipartite graph G_{pq}, we assign each vertex from G_p or G_q at most one matched vertex from the other graph G_q or G_p. Unfortunately, the Hungarian algorithm usually requires expensive computation and thus may lead to computational inefficiency for the depth-based matching. To address this inefficiency, an alternative way or strategy is to randomly assign each vertex an unique matched vertex through the correspondence matrix C. In other words, in the correspondence matrix C, from the first row and the first column or from the first column and the first row, we will set each evaluating element of C to 0 if there has been an existing element that is 1 either in the same row or the same column. This strategy will not influence the effectiveness of our resulting kernel in Section 6, and the kernel is more efficient than that using the Hungarian algorithm.

5.2 Hypergraph Matching Based on Coarse Feature Correspondences

The first-order feature matching that identifies the correspondence between vertices of graphs does not reflect the information converged by the vertex coordinates in the EUS images. As a result, it does not take into account the relative position between vertices in the graphs in terms of the coordinates of the EUS images. However, in the literature, coordinate information is usually

important for precisely aligning vertex correspondences, i.e., one can identify incorrect matches between graphs through coordinate information.

To address this problem, we seek to develop a high-order graph matching framework (referred to as hypergraph matching) for refining feature correspondences between two EUS images. Unlike first-order feature point matching methods which neglect the spatial correlations of feature points, we encode spatial proximity relations into hyperedges, so as to match the edges or triangles between two graphs. This will better preserve the geometry within each graph and as a result the matching results will be more stable. The high-order graph matching method works under the translation, rotation, reflection and even strong deformation of either graph. Therefore, it is more likely to identify mismatches in the coarse matching results and recover meaningful matching between graphs. Moreover, this method allows us to choose different potential functions to incorporate prior knowledge of the graphs and easily generalizes to higher order matching.

Based on the definitions in Eq.(4), Eq.(5) and Eq.(6), we compute the correspondence matrix C. The correspondence matrix C records the matched vertex pairs between EUS images. Supposed the M first-order feature points are denoted as $p_1, \ldots, p_M$ in the EUS image1 which are matched with M feature points denoted as $q_1, \ldots, q_M$ in the EUS image2, respectively. We then use the hypergraph matching strategy to refine the feature matching results obtained in Section 5.1. We use the set of M feature points in the EUS image1 to form a uniform hypergraph HG_p where the vertices represent the feature points in the EUS image1 and the weight on its one hyperedge measures the spatial relationship among K vertices. In our work, we use three vertices (i.e., K=3) to form one hyperedge. Let $\mathcal{A}$ be the adjacency tensor for the hypergraph HG_p with its (i, j, k)th entry $a_{i,j,k}$ representing the weight on the hyperedge is determined by

$$a_{i,j,k} = U(p_i, p_j, p_k) \cdot W(p_i, p_j, p_k) \tag{7}$$

where i, j, k are the indices of the vertices p_i, p_j, p_k in the hypergraph HG_p. We define $U(p_i, p_j, p_k)$ and $W(p_i, p_j, p_k)$ of (7) respectively as

$$U(p_i, p_j, p_k) = \det([v_i - v_k, v_j - v_k]) \tag{8}$$

and

$$W(p_i, p_j, p_k) = \sum_{i,j,k} \frac{1}{\sqrt{||v_i - v_k|| \cdot ||v_j - v_k||}} \tag{9}$$

where the two dimensional column vectors v_i, v_j, v_k represent the coordinates of the vertices p_i, p_j, p_k. The relation in Eq.7 defines the high-dimensional sine function for the multiple angles established by p_i, p_j and p_k in the hyperplane [8]. For a sole angle in a plane, Eq.7 reduces to the normal definition for sine. Here we use the high-dimensional sine function to characterize the higher-order correlation within an n-tuple. Furthermore, we use it as hyperedge features

for measuring hyperedge similarity. If two n-tuples are structurally similar, their high-dimensional sine function is supposed to be close. Therefore, the value of $a_{i,j,k}$ equals to zero if there is no hyperedge encompassing p_i, p_j, p_k. According to Eq.7, the value of $a_{i,j,k}$ is large when the three vertices are close geometrically, and is small if these vertices are geometrically different [17].

Fig. 5 shows the hypergraphs and the matching example for two EUS images.

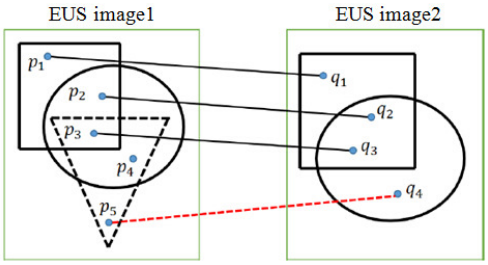

Fig. 5 Matching example for EUS images. Different shape of borders represent hyperedges of each hypergraph. Additionally, the solid line and the dash line between feature points represent correct match and incorrect match, respectively.

From the hypergraph HG_p and HG_q, we establish an association hypergraph HG, whose M vertices represent the possible matching pairs between EUS images and the weight on its hyperedge measures the similarity of the potential correspondences. We build the adjacency tensor $\mathcal{S}$ for HG with (i,j,k)th entry $S_{i,j,k}$ representing the hyperedge weight, which is defined as follows

$$S_{i,j,k} = \exp[-\frac{\|a_{i,j,k} - b_{i,j,k}\|_2^2}{\sigma}] \tag{10}$$

where σ is a scaling parameter. Fig. 6 shows the association hypergraph HG for the hypergraph structures in Fig. 5.

According to (10), $S_{i,j,k}$ characterizes the similarity between one form (i.e., a hyperedge encompassing feature points $\{p_i, p_j, p_k\}$) in HG_p and the matched hyperedge encompassing the matched feature points $\{q_i, q_j, q_k\}$ in HG_q. Additionally, it characterizes the structural consistency between the hypergraphs established based on EUS image1 and EUS image2 separately.

5.3 Structural Refinement for First-order Feature Point Matching Results

The task of structurally refining the first-order feature point matching results can be transformed into removing outliers, i.e., the incorrect matching results, from a tight cluster in the subspace spanned by the adjacency tensor $\mathcal{S}$ of the association hypergraph HG. According to Ren *et al.* [16], we apply variations of dominant cluster analysis (DCA) for High Order Dominant Cluster

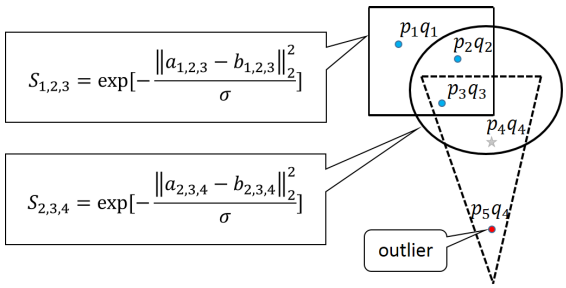

Fig. 6 The association hypergraph for the hypergraphs in Fig. 5. Four round form in blue represent the initial matching pairs and the one starlike form in gray represents the correct matching pair which is not established.

Analysis (HO-DCA), removing outliers. We denote the column vector $\mathbf{x}$ to record the matching score, whose nth entry x_n (n=1, ..., M) indicates the degree of structural consistency for the potential matching pairs $\{p_n, q_n\}$. Let $\mathbf{T}$ denote the subset of vertices in HG which represent the correctly matched pairs of vertices from HG_p and HG_q. As a result, the nth entry x_n of $\mathbf{x}$ also represent the probability for the nth vertex in HG belong to $\mathbf{T}$. For our three-dimensional tensor by using these ingredients, the optimal model can be formulated as

$$\widehat{\mathbf{x}} = \arg\max_{\mathbf{x}} \sum_{i=1}^{M}\sum_{j=1}^{M}\sum_{k=1}^{M} S_{i,j,k} \prod_{n=i,j,k} x_n \tag{11}$$

subject to the constraints $\forall n$, $x_n \geq 0$ and $\sum_{i=1}^{M} x_i$=1.

According to (11), if the initial matching pair $\{p_n, q_n\}$ is an incorrect matching pair of $\mathbf{T}$, then the nth entry x_n of $\mathbf{x}$ will much less than 1. We refer to the nonzero value x_n satisfying the optimality condition in (11) as the association degree for the matching pair $\{p_n, q_n\}$. Therefore, the problem of removing outliers can be posted as a constraint optimization problem.

According to [16], we adopt the following iterative formula to update x_i to convergence

$$x_i(t+1) = x_i(t) \frac{\sum_{j=1}^{M}\sum_{k=1}^{M} S_{i,j,k} \prod_{n=j,k} x_n(t)}{\sum_{i=1}^{M}\sum_{j=1}^{M}\sum_{k=1}^{M} S_{i,j,k} \prod_{n=i,j,k} x_n(t)} \tag{12}$$

where t indicates the tth iteration. The remaining M-1 entries of $\mathbf{x}$ can be computed in the same iterative formula (12).

We use (12) to update the score vector $\mathbf{x}$ until we reach convergence. At convergence the score vector $\mathbf{x}$ is the optimal solution to (11) and the nonzero elements in $\mathbf{x}$ corresponds to correct matches.

5.4 Computational Complexity

We consider the problem of matching two K-uniform hypergraphs each having N vertices. The existing hypergraph matching strategies establish an association hypergraph with N^2 vertices by enumerating all potential matching pairs and $\mathrm{C}_{N^2}^K$ hyperedges. Normally, these strategies are not feasible for practical applications, because they have the computational complexity $O((N^K)^2)$. This is especially when the value of N and K are large. In contrast, our hypergraph matching framework establishes an association hypergraph with only N vertices and C_N^K hyperedges. The computational complexity of our method is $O(N^K)$. Key to this efficiency is that the feature-based matching establishes coarse correspondences between the hypergraphs HG_p and HG_q, and thus significantly reduces the enumeration of possible matching pairs. Thus, our hypergraph matching framework improves the matching accuracy by discarding outliers from the coarse matching results with low computational complexity.

6 A new high-order graph matching kernel for SVM classifier

We use the first-order and high-order graph matching strategies that are described in previous sections, and define a new graph kernel function by counting the number of matched vertex pairs. Consider $G_p(V_p, E_p)$ and $G_q(V_q, E_q)$ as a pair of sample graphs. Based on the definitions in Eq.(10), Eq.(11) and Eq.(12), we compute the score matrix $\mathbf{x}$, where the nonzero elements in $\mathbf{x}$ corresponds to correct matches. The resulting graph matching kernel value $k(G_p, G_q)$ between $G_p(V_p, E_p)$ and $G_q(V_q, E_q)$ is computed by counting the number of nonzero elements of $\mathbf{x}$.

For a graph dataset having N graphs, the kernel matrix can be computed using the following computational steps: 1) For each graph, compute the h-layer depth-based representation around each vertex; 2) Compute the initial corresponding matrix C for each pair of graphs based on their depth-based representations; 3) Refine the matching results by hypergraph matching; 4) Compute the kernel value for each pair of hypergraphs based on the number of nonzero elements in $\mathbf{x}$. When the kernel matrix obtained, we can use it to train a support vector machine (SVM) classifier.

7 Experiments and Comparisons

A 10-fold cross-validation strategy is employed to evaluate the classification performance. Specifically, the entire sample is randomly partitioned into 10 subsets and then we choose one subset for test and use the remaining 9 for training, and this procedure is repeated 10 times. The final accuracy is computed by averaging of the accuracies from all experiments. We quantify classification performance using four statistical measures, i.e., accuracy, sensitivity, specificity, and the area under the receiver operating characteristic curve (AUC).

7.1 Cluster Evaluation

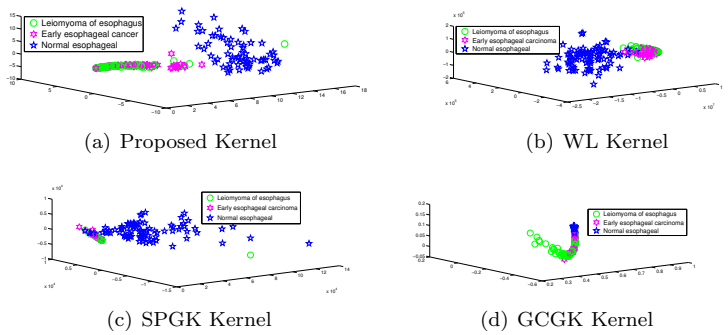

(a) Proposed Kernel (b) WL Kernel

(c) SPGK Kernel (d) GCGK Kernel

Fig. 7 Distribution of samples of three types of esophageal EUS images using the leading three principal components extracted from kernel ECA.

First, we evaluate the performance of our proposed kernel on graph clustering problems. We also compare our kernel with several alternative state of the art graph kernels. These graph kernels include 1) the Weisfeiler-Lehman subtree kernel (WL) [38], 2) the shortest path graph kernel (SPGK) [39], and 3) the graphlet count graph kernel (GCGK) [40]. For our kernel, we set h as 10. For the WL kernel, we set the highest dimension (i.e. the highest height of subtrees) of the Weisfeiler-Lehman isomorphism as 10. For the GCGK graph kernel, we set the size of a graphlet as 3. For each kernel, we perform the kernel entropy component analysis (kECA) [25] on the kernel matrix to embed graphs into a 3-dimensional principal space. From Figure 7, it is clear that our method demonstrates much clearer cluster structure than that by other three alternative kernel methods, with relatively little overlap between clusters. Form Figure 7(a), different dispersions were obtained for each cluster, with the non lesions of esophageal EUS images giving the largest scatter and the remaining two types of esophageal lesions (leiomyoma and early carcinoma) yielding relatively compact clusters. Form Figure 7(a), there is a separation of early esophageal carcinoma from leiomyoma of esophagus, with early esophageal carcinoma tending toward the right of the figure and leiomayoma from left. However, there still exists some overlap between them, which is largely a consequence of the projection of the data onto a three dimensional space and could be minimized by considering a higher dimensional space.

7.2 Classification performances

The confusion matrix for the three groups, provided in Figure 8, shows that the system performs very well on healthy images of the esophagus, since more

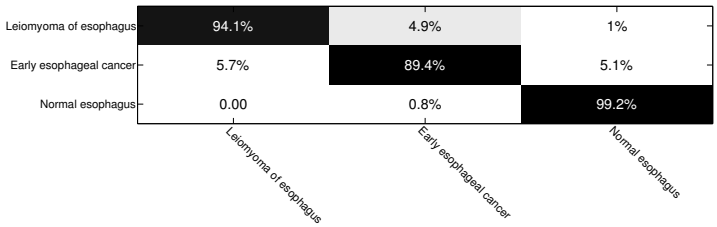

Fig. 8 The confusion matrix for EUS image classification

than 99% of healthy images have been correctly classified. The false alarm rate, i.e. healthy patients mistaken for early esophageal carcinomas, is quite small. However, non-detection, i.e., early esophageal carcinoma subjects mistaken for healthy ones, represent a greater risk than false alarms. This non-detection rate, which reaches 5.1% for the early esophageal carcinoma group, leaves room for improvement. In order to fully evaluate the proposed method for the early detection of this type of disease in esophagus, the sensitivity, specificity, positive predictive value (PPV), negative predictive value (NPV) and the overall diagnostic accuracy were calculated (see Table 1). Sensitivity measures the proportion of actual positives which are correctly identified (e.g. the percentage of early esophageal carcinoma patients who are identified as having the condition), and the specificity measures the proportion of negatives which are correctly identified (e.g. the percentage of normal subjects who are identified as none suffer from any esophageal disease). As shown in Table 1, the proposed method yields an excellent testing performance of 93% accuracy on average, for multiple computer runs of the new SVM model. Specifically, in the case of early esophageal carcinoma, the classification had a sensitivity of 94% which is clinically important for early and proper treatment. The specificity is 95%, positive predictive value is 89% and negative predictive value of 97%. Figure 9 shows the corresponding bi-normal receiver operating characteristic (ROC) curves for three cases. The diagonal reference line represents the outcome of a test that offers no predictive benefit and has an area under the curve of 0.5. The area under all the three ROC curves close to 1 indicating a very good classification performance.

Table 1 Performance characteristics of the SVM classifier with new kernel

	Sensitivity	**Specificity**	**PPV**	**NPV**
Leiomyoma	94%	97%	94%	97%
Early carcinoma	94%	95%	89%	97%
Normal	94%	100%	99%	97%
		Overall	**accuracy:**	93%

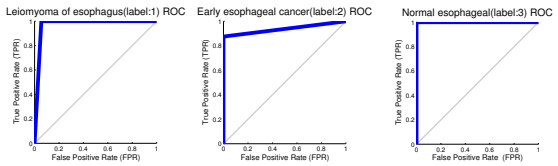

Fig. 9 Receiver operating characteristic (ROC) curve for differential diagnosis of leiomyoma, early esophageal carcinoma and normal esophagus by using a new SVM model

To provide a better evaluation of proposed approach, a comparison with traditional texture analysis algorithm was performed. The algorithm for reference is Tamura [26]. Tamura gives five textural properties: Coarseness, Contrast, Directionality, Line-Likeness and Regularity. Coarseness basically relates to the distance in gray levels of spatial variations, which is implicitly related to the size of primitive elements forming the texture. Contrast measures distribution of graph levels that varies in an EUS image and to what extent its distribution is biased to black or white. Directionality of an EUS image is measures by the frequency distribution of oriented local edges against their directional angles. Line-Likeness in an EUS image is average coincidence of direction of edges that co-occurred in the pairs of pixels separated by a distance along the edge direction in every pixel. Regularity measures a regular pattern or similar that occurred in an EUS image. The experiment results are listed in Table 2. From Table 1 and Table 2, we can conclude that our proposed method is more competent than Tamura features in texture analysis no matter using any values to figure the performance.

Table 2 Performance characteristics of the SVM classifier with Tamura texture features

	Sensitivity	**Specificity**	**PPV**	**NPV**	**Accuracy**
Tamura	82%	85%	75%	89%	65%

8 Discussion

The incidence of gastrointestinal malignant carcinoma is increasing with population, therefore the diagnosis of gastrointestinal carcinoma become very important for the prognosis of patients, this is especially for the patient with erly gastrointestinal carcinoma. However, early diagnosis remains a significant clinical challenge to medical doctors, in particularly in the setting of the prognosis of gastrointestinal malignant carcinoma [34]. EUS is an important medical method for the judgement of early gastrointestinal carcinoma, it can provide accurate staging of associated lesions [35,36]. However, the decision of

EUS are affected by many factors. Published studies reported that even with the application of EUS-FNA and biopsy, the sensitivity in diagnosing gastrointestinal malignant carcinoma was still very low. When there is coexistence of pancreas and gall bladder lesions or masses, leiomyoma, the sensitivity was even lower. This decrease in sensitivity can be caused by many subjective or objective variables associated with increased cytologic yield from EUS, such as experience of doctors, the resolution ability of medical equipment, the tumor size and staging. In addition, for the endoscopic ultrosonography (EUS) physician, the ability to identify the different early gastrointestinal carcinoma is also crucial. Interpretation of EUS images is inherently subjective and depends on the endoscopist's experience. If the biopsy results cannot provide effective support, the medical process will be tough for both patients and doctors. The image classification of early gastrointestinal carcinoma is the core of diagnosis [37]. Although noninvasive US tissue characterization could address this issue and reduce the need for repeated biopsies, this method still seems to be limited by its poor quantification capability. To overcome these limitations, we have attempted to derive more objective findings from EUS images.

A EUS image is composed of pixels, and its echo density is expressed in brightness values from 0 (black) to 255 (white). The texture analysis of EUS images is, in principle, a technique for evaluating the distribution and spatial variation of the pixel intensities [31]. Texture features are helpful for classifying lesions in sonography [32], and the potential of sonographic texture analysis to improve tumor diagnosis has already been demonstrated[2,3]. Because most of these diagnostic features are related to the textural properties of the EUS images, they can be investigated in a quantitative and systematic way via automated texture extraction and analysis directly from the digitized EUS image. In our study, we present a novel method for extracting texture information. If input EUS image is converted into an undirected graph whose vertices correspond to the SIFT features. Then, we compute an h-layer depth-based representation for a graph, which is effected by measuring the Shannon entropies of a family of K-layer expansion subgraphs derived from a vertex of the graph. The depth-based representations characterize graphs in terms of high dimensional depth-based complexity information. This enables us to perform a texture analysis which considers both micro and macro texture information. The present study have proved that analysis of the texture information of EUS image allows the differentiation between early esophageal carcinoma and leiomyoma of the esophagus with a good sensitivity, specificity, and accuracy.

Kernel-based methods such as support vector machines (SVM) have been used as a potential mechanism for the design of a classifier responsible for differentiating between malignant and begin lesions[33]. Compared to alternativer classifier paradigms, such as neural networks, fuzzy classifiers, or decision trees, SVMs (which are based on the principle of structural risk minimization) offer advantages, such as a convex objective function with efficient training algorithms and good generalization properties. However, they are rather limited for processing complex structured data such as EUS images when used with stan-

dard kernels such as the Gaussian kernel applied to global features. The key contribution of this paper is the definition of a new kernel for SVM approach based on graph matching for EUS images. Our kernel keep the underlying topological structure of graphs by describing them through the depth-based representation and high-order graph matching. Moreover our kernel encompasses local information, by computing the depth-based representation around a vertex by measuring a Shannon entropy for this expansion subgraph. It also encapsulates global information, by gauging the Shannon entropy flow using the expansion subgraphs. It thus reflects the high dimensional complexity characteristics of the graph around the vertex. This implies that our proposed kernel matrix can encode more structured information from EUS images.

By computing the SVM classifier with a new kernel, we obtained a good overall testing performance (93%), used for the differential diagnosis of early esophageal carcinoma, leiomyoma of esophagus and normal esophagus. Moreover, the area under each ROC curve was close to 1, which indicated excellent values of sensitivity, specificity, and accuracy for this imaging approach for the differential diagnosis of early esophageal carcinoma, leiomyoma of esophagus and normal esophagus. This is essential in borderline cases, in which the value of EUS-FNA is limited by the low sensitivity. Because EUS-FNA in patients with focal esophageal lesions has a low NPV, the utility of a neural computing approach of EUS elastography recordings cannot be underestimated.

The establishing of gastrointestinal early carcinoma image classification recognition system is just a starting of the understanding of all gastrointestinal diseases by EUS. We have attempted to recognize the features of gastrointestinal diseases from different perspective. According to its preliminary results of testing, the image classification system is effective for diagnosis of early gastrointestinal carcinoma, however lots of further work still need to be done. This includes increasing sample libraries, improving the identification accuracy of the image classification recognition system, and clinical application testing are equally important for the modification, and if permitted, we may also be able differentiated the Crohn's disease, intestinal tuberculosis, White plug's diseases and the intestinal lymphoma using our system.

9 Conclusion

In this paper, a hypergraph matching framework for refining first-order feature correspondences has been proposed. The framework we presented jointly considers both feature similarities and spatial feature layouts. Our framework takes first-order feature point matching results as a coarse matching. Then we have conducted hypergraph matching for rejecting mismatches and thus obtained refined correspondences. Our framework has exhibited effectiveness in differentiating between normal, leiomyoma of esophagus and early esophageal carcinoma. Furthermore, our method is computationally efficient because the association hypergraphs established based on coarse correspondences have a considerable smaller number of vertices than hypergraph based

matching methods without the coarse matching. Quantitative evaluation in our experiments has shown that our method achieves high accuracy.

Acknowledgements This work is supported by National Natural Science Foundation of China (Grant No.61402389), Fundamental Research Funds for Central Universities (No. 15CX05042A) and Shandong Outstanding Young Scientist Fund (No. BS2013DX006).

References

1. Kolios MC, Czarnota GJ, Lee M, Hunt JW, Sherar MD (2002) Ultrasonic spectral parameter characterization of apoptosis. Ultrasound Med Biol 28: pp. 589-597.
2. Van HC, Van CB, Valentin L et al. (2007) External validation of mathematical models to distinguish between benign and malignant adnexal tumors: a multicenter study by the International Ovarian Tumor Analysis Group. Clin Cancer Res 13: pp. 4440-4447.
3. Van HC, Van CB, Valentin L et al. (2009) Prospective internal validation of mathematical models to predict malignancy in adnexal masses: results from the international ovarian tumor analysis study. Clin Cancer Res 15: pp. 684-691.
4. Norton ID, Zheng Y, Wiersema MS, Greenleaf J, Clain JE, Dimagno EP (2001) Neural network analysis of EUS images to differentiate between pancreatic malignancy and pancreatitis. Gastrointest Endosc 54: pp. 625-629.
5. Das A, Nguyen CC, Li F, Li B (2008) Digital image analysis of EUS images accurately differentiates pancreatic cancer from chronic pancreatitis and normal tissue. Gastrointest Endosc 67: pp. 861-867.
6. Sftoiu A1, Vilmann P, Gorunescu F, Gheonea DI, Gorunescu M, Ciurea T, Popescu GL, Iordache A, Hassan H, Iordache S (2008) Neural network analysis of dynamic sequences of EUS elastography used for the differential diagnosis of chronic pancreatitis and pancreatic cancer. Gastrointest Endosc 68(6): 1086-1094.
7. Bai L, Hancock ER (2014) Depth-based complexity traces of graphs. Pattern Recognition 47(3): 1172-1186.
8. Eriksson F (1978) The law of sines for tetrahedra and n-simplices. Geometriae Dedicata 7(1): 71-80.
9. Loren DE, Seghal CM, Ginsberg GG et al. (2002) Computer-assisted analysis of lymph nodes detected by EUS in patients with esophageal carcinoma. Gastrointest Endosc 56: pp. 742-746.
10. Olowe K, Kumon R, Farooq FT et al. (2007) Differentiation of benign and malignant lymph nodes by endoscopic ultrasound (EUS) spectrum analysis. Gastrointest Endosc.
11. Noble WS (2006) What is a support vector machine? Nat Biotechnol 24: pp. 1565-1567.
12. Scott GL, Longuett-Higgins HC (1991) An algorithm to associating the features of two images, In: Proc. the Royal Society of London B, 244: pp. 313-320.
13. Zhang M, Yang H, Jin Z, Yu J, Cai Z, Li Z (2010) Differential diagnosis of pancreatic cancer from normal tissue with digital imaging processing and pattern recognition based on a support vector machine of EUS images. Gastrointest Endosc, 72(5): pp. 978-985.
14. Zhu M, Xu C, Yu J, Wu Y, Li C, Zhang M, Jin Z, Li Z (2013) Differentiation of Pancreatic Cancer and Chronic Pancreatitis Using Computer-Aided Diagnosis of Endoscopic Ultrasound (EUS) Images: A Diagnostic Test. PLOS ONE, 8(5): 1-6.
15. Tuceryan M, Jain AK (1993) Texture analysis. Handbook of Pattern Recognition and Computer Vision, pp.235-276.
16. Ren P, Wilson RC, Hancock ER (2011) High Order Structural Matching Using Dominant Cluster Analysis. In: Internat. Conf. on Image Analysis and Processing (ICIAP), pp.1-8.
17. Lerman G, Whitehouse JT (2009) On d-dimensional d-semimetrics and simplex-type inequalities for high-dimensional sine functions. J. Approximation Theory, 156: pp. 52–81.
18. Julesz B (1975) Experiments in the visual perception of texture. Scientific American, 232(4):34-43.
19. Lowe DG (2008) Distinctive image features from scale-invariant key points. International journal of computer vision 60(2):91-110.

20. Shannon, Claude E (1948) A mathematical theory of communication. Bell System Technical Journal 27(3):379423.
21. ärtner TG, Flach PA, Wrobel S (2003) On graph kernels: hardness results and efficient alternatives. In: Proc. COLT, pp.129-143.
22. Jebara T, Kondor RT, Howard A (2004) Probability product kernels. Journal of Machine Learning Research 5: pp. 819-844.
23. Harchaoui Z, Bach F (2007) Image classification with segmentation graph kernels. In: Proc. CVPR.
24. Chang CC, Lin CJ (2011) LIBSVM: A library for support vector machines, Software available at http://www.csie.ntu.edu.tw/ cjlin/libsvm.
25. Jenssen R (2010) Kernel entropy component analysis. IEEE Transactions on Pattern Analysis and Machine Intelligence 32(5):847-860.
26. Tamura H, Mori S, Yamawaki T, Mehlhorn K (1978) Textural features corresponding to visual perception. IEEE Transactions on Systems, Man and Cybernetics 8(6): 460-473.
27. Fontoura Costa L. da, Junior RMC (2000) Shape analysis and classification, Theory and Practice.
28. Bai L, Ren P, Bai X, Hancock ER (2014) A graph kernel from the depth-based representation. In: Proceedings of S+SSPR, pp. 111.
29. Bai L (2014) Information Theoretic Graph Kernels, PhD Thesis, University of York.
30. Munkres J (1957) Algorithms for the assignment and transportation Problems. Journal of the Society for Industrial and Applied Mathematics 5(1):32-38.
31. Nguyen VX, Nguyen CC, Li B, Das A (2010) Digital image analysis is a useful adjunct to endoscopic ultrasonographic diagnosis of subepithelial lesions of the gastrointestinal tract. J Ultrasound Med 29(9):1345-1351.
32. Kolios MC, Czarnota GJ, Lee M et al. (2002) Ultrasonic spectral parameter characterization of apoptosis. Ultrasound Med Biol 28: pp. 589-597.
33. Levman J, Leung T, Causer P et al. (2008) Classification of dynamic jcontrast enhanced magnetic resonance breast lesions by support vector machines. IEEE Trans Med Imaging 27: pp. 688-696.
34. Nagami Y, Tominaga K, Machida H, Nakatani M et al. (2014) Usefulness of nonmagnifying narrow-band imaging in screening of early esophageal squamous cell carcinoma: a prospective comparative study using propensity score matching. Am J Gastroenterol 109(6):845-854.
35. De Angelis C, Manfre SF, Pellicano R (2014) Endoscopic ultrasonography for diagnosis and staging of pancreatic adenocarcinoma: key messages for clinicians. Minerva medica 105(2):121-128.
36. Pech O, May A, Gunter E, Gossner L, Ell C (2006) The impact of endoscopic ultrasound and computed tomography on the TNM staging of early cancer in Barrett's esophagus. Am J Gastroenterol 101(10):2223-2229.
37. Buskens CJ, Westerterp M, Lagarde SM, Bergman JJ, Ten Kate FJ, Van Lanschot JJ (2004) Prediction of appropriateness of local endoscopic treatment for high-grade dysplasia and early adenocarcinoma by EUS and histopathologic features. Gastrointest Endosc 60(5):703-710.
38. Shervashidze N, Schweitzer P, Leeuwen EJ, Mehlhorn K, Borgwardt KM (2010) Weisfeiler-Lehman graph kernels. Journal of Machine Learning Research 1:1-48.
39. Borgwardt KM, Kriegel HP (2005) Shortest-path kernels on graphs. In: Proc. ICDM, pp.74-81.
40. Shervashidze N, Vishwanathan SVN, Petri T, Mehlhorn K, Borgwardt KM (2009) Efficient graphlet kernels for large graph comparison. Journal of Machine Learning Research 5: pp. 488-495.

Author Biographies
Click here to download Author Biographies: author biography.docx

Zhihong Zhang received his BSc degree (1st class Hons.) in computer science from the University of Ulster, UK, in 2009 and the PhD degree in computer science from the University of York, UK, in 2013. He won the K. M. Stott prize for best thesis from the University of York in 2013. He is now a n assistant professor at the software school of Xiamen University, China. His research interests ar e wide-reaching but mainly involve the areas of pattern recognition and machine learning, partic ularly problems involving graphs and networks.

Lu Bai received the Ph.D. degree from the University of York, York, UK, and both the B.Sc. and M.Sc degrees from Faculty of Information Technology, Macau University of Science and Technology, Macau SAR, P.R. China. He is now a Asistant Professor in School of Information, Central University of Finance and Economis, Beijing, China. His current research interests include structural pattern recognition, machine learning, quantum walks on networks and graph matching, especially in kernel methods and complexity analysis on (hyper)graphs and networks.

Peng Ren received his B.E. in electronic information engineering and M.E. in communication and information systems both from Harbin Institute of Technology, China. He received his Ph.D. in computer science from the University of York, UK. He is currently a professor of pattern recognition with China University of Petroleum. His research interests are structural pattern recognition and discrete optimization methods in computer vision.

Edwin R. Hancock received the B.Sc., Ph.D., and D.Sc. degrees from the University of Durham, Durham, U.K. He is now a Professor of computer vision in the Department of Computer Science, University of York, York, U.K. He has published nearly 150 journal articles and 550 conference papers. Prof. Hancock was the recipient of a Royal Society Wolfson Research Merit Award in 2009. He has been a member of the editorial board of the IEEE TRANSACTIONS ON PATTERN ANALYSIS AND MACHINE INTELLIGENCE, PATTERN RECOGNITION, COMPUTER VISION AND IMAGE UNDERSTANDING, and IMAGE AND VISION COMPUTING. His awards include the Pattern Recognition Society Medal in 1991, outstanding paper awards from the Pattern Recognition Journal in 1997, and the best conference best paper awards from the Computer Analysis of Images and Patterns Conference in 2001, the Asian Conference on Computer Vision in 2002, the International Conference on Pattern Recognition (ICPR) in 2006, British Machine Vision Conference (BMVC) in 2007, and the International Conference on Image Analysis and Processing in 2009. He is a Fellow of the International Association for Pattern Recognition, the Institute of Physics, the Institute of Engineering and Technology, and the British Computer Society. He was appointed as the founding Editor-in-Chief of the Institute of Engineering & Technology Computer Vision Journal in 2006. He was a General Chair for BMVC in 1994 and the Statistical, Syntactical and Structural Pattern Recognition in 2010, Track Chair for ICPR in 2004, and Area Chair at the European Conference on Computer Vision in 2006 and the Computer Vision and Pattern Recognition in 2008. He established the energy minimization methods in the Computer Vision and Pattern Recognition Workshop Series in 1997.

Author Photographs
Click here to download Author Photographs: renamed_cb830.jpg

Author Photographs
Click here to download Author Photographs: lubai.jpg

Author Photographs
Click here to download Author Photographs: edwin.jpg

Author Photographs
Click here to download Author Photographs: peng.jpg